Post Access Report

San Juan Islands Tidal Energy Characterization

Awardee: Orbital Marine Power

Awardee point of contact: Oliver Wragg

Facility 1: Pacific Northwest National Laboratory

Facility point of contact: Zhaoqing Yang

Facility 2: University of Washington

Facility point of contact: Brian Polagye

Date: 4/24/2024

TEAMER
Testing & Expertise for Marine Energy

EXECUTIVE SUMMARY

The San Juan Islands are an archipelago with multiple, energetic tidal channels that could be suitable for tidal turbines. At present, there is limited electrical generation on the islands, with power primarily provided by a subsea cable connection with the mainland. The objective of this technical assistance was to evaluate the potential for tidal energy development in the region, based on model results and measurements of tidal currents, as well as site characteristics (geometry and bathymetry). This would allow Orbital Marine Power, the local utility (Orcas Power and Light Company - OPALCO), and other site developers to identify the promising opportunities for tidal energy generation in the San Juan Islands.

University of Washington re-analyzed acoustic Doppler current profiler (ADCP) data at 46 stations in the U.S. waters of the Salish Sea that were collected by NOAA's National Ocean Survey (NOS) CO-OPS program in 2017. To evaluate the power potential for floating tidal turbines, data went through a series of quality assurance checks and then were re-referenced to the sea surface. Over the 46 stations, 13 were excluded from analysis due to water depth or fundamental issues with data quality (e.g., blow down of moored instruments during strong currents). Of the remaining sites, the four with the highest tidal energy potential are:

- NOS Site 40: Bellingham Channel (time-average power density 1.20 kW/m^2)
- NOS Site 32: Western Rosario Strait (time-average power density 1.15 kW/m^2)
- NOS Site 39: Southern Bellingham Channel (time-average power density 1.02 kW/m^2)
- NOS Site 19: Spieden Channel (time-average power density 0.81 kW/m^2)

Of these sites, Orbital Marine Power had expressed particular interest in NOS Sites 19 and 32. For two other areas of interest, measurement data were not available. The NOS survey did not include locations in the San Juan Channel and the mooring deployed in Cattle Pass experienced too much motion to pass quality checks. Of the two sites of interest with measurement data, current profiles were relatively blunt, with limited directional variation over the water column.

PNNL substantially refined the hydrodynamic model grid in the San Juan Archipelago region and conducted two month-long simulations in summer 2017 using 40 sigma layers in the vertical direction. The refined model shows a slightly improved performance in simulating tidal currents compared to the previous modeling study (Yang et al., 2021). The model output includes two type of solution files, high-frequency (12-minute) water level and velocity time series output at >1,700 high velocity sites throughout the San Juan Archipelago and hourly computational grid output that includes additional hydrodynamic parameters (e.g., vorticity, turbulence) covering the entire Archipelago. Specifically, 12-minute time series output was shared with the UW project team for detailed model-data comparisons of current and power density profiles. The computational grid output was used to assess domain-wide hydrodynamic properties that were not captured by NOS surveys.

Overall, this study suggests that there are multiple sites that are likely technically viable for tidal energy generation in the San Juan Islands. The appreciable differences between modeled and measured power density demonstrate the importance and difficulty of validating models in energetic locations, but, at the same time, modeling indicates that measurements were not acquired at locations with the highest power density. In addition to this report, the project team published a journal paper that characterized the differences between power output from seabed and surface-deployed deployed turbines in the San

Juan Islands, as well as the accuracy and appropriateness of different approaches to extrapolating current profiles over the water column.

1 INTRODUCTION TO THE PROJECT

The San Juan Islands are an archipelago with multiple, energetic tidal channels that could be suitable for tidal turbines. At present, there is limited electrical generation on the islands, with power primarily provided by a subsea cable connection with the mainland. The objective of this technical assistance is to evaluate the potential for tidal energy development in the region, based on model results and measurements of tidal currents, as well as site characteristics (geometry and bathymetry). This will allow Orbital Marine Power, the local utility (Orcas Power and Light Company - OPALCO), and other site developers to identify the promising opportunities for tidal energy generation in the San Juan Islands.

Due to the complex geometry and inter-connected waterways, tidal currents around San Juan Islands exhibit strong spatial asymmetry and temporal variability. Therefore, it is important to evaluate available data through a lens of tidal energy, with consideration to metrics such as the power density, vertical shear, and directional asymmetry between ebb and flood tide, and spring and neap tides. Both measurement and simulation data are available for such an analysis, which will incorporate tidal energy site characterization procedures recommended by the International Electrotechnical Commission Technical Specification 62600-201.

Recently, as part of a periodic re-survey to verify tidal current predictions, NOAA's CO-OPS program collected acoustic Doppler current profiler (ADCP) data at 132 stations in the U.S. waters of the Salish Sea from May 2015 to August 2017. Each survey covered a period of 1 - 3 months and 42 stations were located in the San Juan Islands and adjacent waterways. These data, which consist of ~5 minute averages of velocity profiles over 30 – 90 day periods, are available through the CO-OPS web portal and have also been provided in raw form to the University of Washington (UW) for analysis.

Similarly, Pacific Northwest National Laboratory (PNNL) has recently developed a tidal hydrodynamic model for tidal energy resource characterization and assessment in the Salish Sea, with a grid resolution of 50 m – 200 m in the tidal channels (Yang *et al*. 2021). Under this support, PNNL's model was further refined to accurately simulate currents in the San Juan Island domain to account for sharp bathymetry gradients and small channel width. In addition metrics that could be evaluated from ADCP data, the model was used to assess field quantities, such as eddy vorticity, and evaluate spatial gradients at sites of interest.

2 ROLES AND RESPONSIBILITIES OF PROJECT PARTICIPANTS

2.1 APPLICANT RESPONSIBILITIES AND TASKS PERFORMED

Orbital Marine Power worked with UW and PNNL to develop a list of metrics relevant to understanding the economic feasibility of the specific sites. Orbital Marine Power reviewed analysis and simulation results from UW and PNNL to ensure that they met Orbital Marine Power's development needs and, using power curve information, estimated annual energy production for the O2 turbine platform at sites with favorable currents, water depth, and cross-section area.

2.2 Network Facility Responsibilities and Tasks Performed

UW analyzed ADCP data from the stations that NOAA CO-OPS surveyed in April - August, 2017 in the San Juan Islands. This analysis provided insight into the characteristics of tidal currents throughout the archipelago and served as validation data for the more comprehensive modeling effort undertaken by PNNL.

PNNL refined their Salish Sea tidal hydrodynamic model in the San Juan Islands region and simulated the tidal circulation for the period corresponding to the NOAA CO-OPS ADCP data (April - August, 2017). To produce model output used for this study, two standalone, month-long hydrodynamic model simulations (4/25/2017–5/25/2017, 6/25/2017–7/25/2017) were conducted in summer 2017. Both simulations shared the same model configuration except they cover different time windows, assuring a minimum of month-long coverage for all 46 NOS ADCP survey sites in the San Juan archipelago. Validation was against water level, velocity profiles, and tidal energy metrics for periods with available measurement data. The validated model was used to generate a series of hydrodynamic parameters such as tidal currents, power density gradients for selected transects, turbulent kinetic energy, and vorticity for the entire San Juan Islands domain. For example, 4-D velocity (time, x, y, and z) and 3-D surface elevation (time, x, and y) fields were archived at hourly interval for the entire computational grid (193,449 vertices and 374,602 elements) in the San Juan archipelago region and at 12-min intervals for more than 1,700 individual high-velocity locations (e.g., including all 46 NOS sites). Specifically, the 12-min model output was used for high-resolution model-data comparisons at NOS sites while hourly computational grid output provides a domain-wide coverage of many more hydrodynamic variables at many additional locations that are not covered by the NOS survey.

3 Project Objectives

Working with OPALCO and PNNL, Orbital Marine Power had identified four sites of particular interest in the San Juan Islands: Spieden Channel, the western margin of Rosario Strait, San Juan Channel, and Cattle Pass. This screening analysis did not include a detailed evaluation of tidal current characteristics, such that this scope represented a logical next step in project development. By evaluating currents at these sites, as well as other locations throughout the San Juan Islands, we provided Orbital Marine Power and OPALCO with critical information about tidal energy feasibility in the region.

As this is a resource characterization study, key parameters include a number of technology-independent quantities. For ADCP data, these included probability distributions of depth-varying current speed and power density and depth-varying directional asymmetry between ebb and floor tide. PNNL simulation output included the same, as well as quantifying turbulent kinetic energy and vorticity, the latter being representative of eddy structures that could affect turbine performance and structural loading. Power density and kinetic energy fluxes across selected transects in the tidal channels were also analyzed. In particular, spatial gradients for resource characteristics (e.g., current magnitude, power density) were calculated at various temporal scales (instantons, tidally, spring-neap and yearly averages).

In addition, the project team developed analogous technology-dependent quantities. These include distributions of current speed and power density, as well as directional asymmetry, at rotor hub height.

From this, Orbital Marine Power would be able to estimate Annual Energy Production (AEP) following IEC 62600-201 and compare this to thresholds for economic viability based on prior project experience.

4 Test Facility, Equipment, Software, and Technical Expertise

University of Washington

Analysis of ADCP data was conducted on basic computer workstations using MATLAB. The project was overseen by Dr. Brian Polagye, who had conducted similar analysis of ADCP data at other potential tidal energy sites in Puget Sound, including Admiralty Inlet and Tacoma Narrows.

Pacific Northwest National Laboratory

Model simulations for this project were conducted at PNNL's Institutional Computing facility (PIC). The modeling component of the project was overseen by Dr. Zhaoqing Yang. The PNNL's modeling team led by Dr. Yang has rich experiences in conducting tidal modeling in many estuaries and coastal bays, including the Salish Sea. Model outputs are in NetCDF format. All data are archived and were made available to the project team for analysis related to the project.

5 Test or Analysis Article Description

Orbital Marine Power's tidal technology is a floating tidal stream energy generator (Figure 1). A cylindrical floating steel superstructure, which houses power conversion and auxiliary systems, provides reference and attachment for two leg structures with nacelles mounted at their ends. The leg structures have hinge attachments to the superstructure such that, with an actuation system, they can be lowered to position the nacelles and contra-rotating rotors in the optimal part of the tidal stream resource to generate power or be raised to bring the legs, nacelles and rotors to the surface for the purpose of servicing and turbine towing. Station keeping is provided to the superstructure via a multi-anchor catenary mooring system consisting of rope tethers, mooring chain and anchors. Power is exported from the turbine via a dynamic cable from the superstructure to the seabed where it connects to seabed static cabling infrastructure that exports power ashore.

The technology has been developed to 2MW, including the world's most powerful tidal turbine, the SR2000 and upcoming O2 2MW. Each turbine rotor is 20-22 m in diameter with the rotor tips submerged 3 m below the water surface at the apex of their rotation.

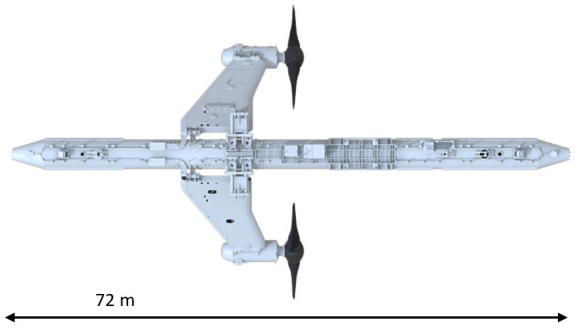

a) Rendering of O2 turbine

b) O2 turbine and mooring system under tow for deployment

Figure 1: O2 turbine overview

6 Work Plan

The project work plan consists of three tasks:

- Task 1 (UW lead): Evaluate ADCP data for all NOAA CO-OPS stations in the San Juan Islands
- Task 2 (PNNL lead): Refine numerical domain within the San Juan Islands, conduct simulation hindcast for the CO-OPS survey period, and analyze data
- Task 3 (Orbital Marine Power lead): Estimate annual energy production at sites of interest

6.1 Numerical Model and Analysis Description

Current measurements or simulation output consists of data at discrete horizontal coordinates and vertical levels. The base quantities are horizontal current velocity ("east" (u) and "north" (v) components) and vertical velocity (w). For ADCP data, because a 6-minute average is generally insufficient to remove all the effects of turbulence, prior to other analysis, we smoothed the data with a 12-minute average. For model data, simulated water level, velocities (u, v, w) and turbulence parameters (KTE, intensity and dissipation rate) were output at every model grid point and vertical layer (for velocity and turbulence quantities).

Instantaneous tidal power density (P_t) is given as

$$P_t = \frac{1}{2}\rho U^3$$

where ρ is the water density and U is the horizontal current speed, calculated as

$$U = \left(u^2 + v^2\right)^{1/2}.$$

Probability distributions of P_t and U can then be calculated, as a function of depth, from time series of velocity. While the instantaneous direction of the currents can be calculated as

$$\theta = \tan^{-1}\left(\frac{v}{u}\right),$$

Principal Component Analysis (PCA) of the horizontal components of currents provides a more reliable estimate of the dominant direction of ebb and flood. From this, currents were classified as “ebb” or “flood” and the average directional deviation between the two calculated. This calculation excludes currents below a slack water threshold value (0.4 m/s) where current direction is more variable, but largely irrelevant in tidal energy applications. Absolute directions were converted to compass coordinates and adjusted for annual variations in declination (deviation between true north and magnetic north). The directional asymmetry (θ_{asym}), defined as the difference in mean direction for ebb and flood relative to a purely bi-directional current with 180 degree offset, was also calculated as a function of depth. This quantity can be relevant to understanding the likelihood of off-axis flow and forces on the mooring.

In addition, the best fit log law for the vertical profile of the current speed was specified through a least squares regression as

$$U(z) = \frac{U^*}{\kappa}\ln\left(\frac{z}{z_o}\right)$$

where U^* is the friction velocity, κ is Von Karman’s constant, and z_o is the surface roughness. Larger values of z_o correspond to a shallower velocity profile, with greater vertical shear. Regressions were performed on populations of velocity profiles defined by their mid-water current speed. This was preferable to fitting vertical profiles for each time step because individual profiles were rarely well-described by this log law and fitting individual profiles was computationally intensive. As discussed in Section 7.1 and 7.2, this form of the vertical profile was not particularly descriptive of sites of interest to Orbital Marine Power.

These quantities and distributions are calculated for all NOAA CO-OPS ADCP stations with valid data and compared to model data at a subset of locations for validation purposes. Model performance for simulated water level and depth-averaged quantities was evaluated using a set of commonly used error statistics, such as root-mean-square-error (*RMSE*), scatter index (*SI*), Bias and linear correlation coefficient (*R*).

The *RMSE* is defined as

$$RMSE = \sqrt{\frac{\sum_{i=1}^{N}(P_i - M_i)^2}{N}}$$

where N is the number of observations, M_i is the measured value, and P_i is the model-predicted value.

The scatter index (*SI*) is the normalized *RMSE* with the average magnitude of measurements:

$$SI = \frac{RMSE}{\overline{|M|}}.$$

The bias (*Bias*) is defined as the mean difference between model predictions and the measurements:

$$Bias = \frac{\sum_{i=1}^{N}(P_i - M_i)}{N} .$$

The linear correlation coefficient (*R*) is a measure of the linear relationship between model predictions and measurements:

$$R = \frac{\sum_{i=1}^{N}\left(P_i - \overline{P}\right)\left(M_i - \overline{M}\right)}{\sqrt{\left(\sum_{i=1}^{N}\left(M_i - \overline{M}\right)^2\right)\left(\sum_{i=1}^{N}\left(P_i - \overline{P}\right)^2\right)}}.$$

As for vertical profile comparison, it is extremely challenging to compare the modeled results and observed data at every 12-min interval because of the large number of time history points (3600 points for 12-min interval over 30 days), comparisons of temporal averages or percentile distribution can be conducted.

Unlike measurement data, which consists of a sparse set of vertical profiles, model data are available throughout the numerical domain. This allows us to calculate additional quantities of interest for tidal energy development.

Turbulence parameters, including turbulence intensity, turbulence kinetic energy and dissipation rate will be directly outputted from the model. Vorticity is defined as the curl of the depth-average or layered horizontal velocity (*u*, *v*) and can be calculated as

$$\omega = \nabla \times V = \frac{\partial v}{\partial x} - \frac{\partial u}{\partial y}.$$

Spatial maps, at both horizontal plane and vertical transects, of power density, turbulence parameters, vorticity, and flood-ebb and time-average directional asymmetries were generated to highlight the spatial gradients at various temporal scales, such as instantaneous flood and ebb tides, tidally, spring-neap period and yearly averages.

All of the above are technology-independent quantities relevant to general development of tidal energy. So that Orbital Marine Power can evaluate the significance of these quantities to the O2 turbine, technology-dependent quantities were also be calculated. Initially, the project team intended to calculate these on the basis of a spatial average over the turbine rotor. However, based on analysis discussed in Calandra et al. (2023), hub-height quantities were shown to be accurate predictors of rotor-averaged values (further discussion in Lessons Learned). Because model results are available throughout the water column, all technology-dependent quantities can be calculated by integrating over the turbine swept area.

For both model and measurement data, we adhere to statistical rules (i.e., spatial and temporal averages of point and instantaneous power density, respectively, rather than computing spatial or temporal averages of velocity and using these to calculate power density).

6.2 TEST AND ANALYSIS MATRIX AND SCHEDULE

	M1				*M2*				*M3*				*M4*				*M5*				*M6*			
Tasks	**WK1**	**WK2**	**WK3**	**WK4**	**WK5**	**WK6**	**WK7**	**WK8**	**WK9**	**WK10**	**WK11**	**WK12**	**WK13**	**WK14**	**WK15**	**WK16**	**WK17**	**WK18**	**WK19**	**WK20**	**WK21**	**WK22**	**WK23**	**WK24**
UW Activity																								
Download ADCP data from NOAA C-MIST portal and organize for analysis																								
Update existing MATLAB codes for batch processing using a single site as a test case																								
Process ADCP data from all sites																								
Visualize and explore tidal energy metrics																								
PNNL Activity																								
Refine numerical simulation for San Juan Islands																								
Calculate tidal energy metrics and compare to measurement analysis																								
Generate spatial maps of tidal energy resources throughout the San Juan Islands																								
Joint Activity: Orbital Marine Power, UW, PNNL																								
Identify most promising sites																								
Calculate annual energy production at most promising sites																								
Joint Publication																								
Post Access Report																								
Post Access Questionnaire																								

6.3 SAFETY

As this project involves only numerical analysis, there are not specific safety protocols beyond the normal operational safety protocols employed by UW, PNNL, and Orbital Marine Power.

6.4 CONTINGENCY PLANS

As CO-OPS ADCP has been provided to the project team and the baseline numerical model has undergone significant technical development and validation, we do not anticipate encountering issues that require contingency plans. In the event that a model quantity diverges from the ADCP measurement data at a location, we will caveat this uncertainty in any spatial maps that are derived from that quantity. Although significant deviations of AEP were observed for model-data comparisons at two of the four sites examined in this study, model results showed similar trend to the measurements and mean velocity deviations were within 15% range. Model-data deviations were quantified and reported. Model accuracy can be improved by updating the model bathymetry with new and accurate survey data.

6.5 DATA MANAGEMENT, PROCESSING, AND ANALYSIS

6.5.1 Data Management

MHK-DR submissions are summarized in Table 1.

ADCP data and quantities calculated from it are stored on workstations at UW and mirrored to network-attached storage. Processed data are be stored in .mat format, with one file per site. Each file contains the following data:

- Location of measurement (latitude and longitude)
- Common name for location of measurement (e.g., “east side of Blakely Island”)
- Dates of measurement
- Current speed probability distributions in 0.1 m/s increments as a function of depth
- Power density probability distributions in 0.1 kW/m^2 increments as a function of depth
- Mean and standard deviation of direction of ebb and flood currents as a function of depth
- Time series of hub-height current speed and direction
- Probably distributions of hub-height power density in 0.1 kW/m^2
- Time series of surface roughness and shear velocity as a function of depth, as well as diagnostic quantities

These .mat files were submitted to MHK-DR, along with a summary table including all sites and a readme file describing the variable names.

Model data, both directly simulated and derived, will be stored in the PNNL project record system and uploaded to MHKDR. All data will be in NetCDF or ASCII format.

For reasons of commercial sensitivity, AEP calculated by Orbital Marine Power was not submitted to MHK-DR.

Table 1: MHK-DR submission summary

Underlying data type	Submission	Submission format
ADCP measurement	Turbine-independent and turbine-dependent data products for each site with valid NOAA CO-OPS data	.mat files for each site .txt readme file describing variables .xlsx summary table (Table 3)
FVCOM model	Tidal hydrodynamic data (water level, velocity and turbulence) and derived energy related data for the entire model domain and simulation period	NetCDF and ASCII files for the entire model domain for the simulation period

6.5.2 Data Processing

We refer to measurement sites with a two-digit site number derived from the formal CO-OPS designation of "PUG17XX" where XX is the site number. ''PUG'' is shorthand for Puget Sound, and ''17'' denotes the survey year (2017). At each site, an upward-facing acoustic Doppler current profiler (ADCP) was deployed for two to four months. The ADCPs collected six-minute ensembles of current speed and direction at discrete increments in the water column (''bins''), capturing vertical variations in the velocity profile over time. Water pressure and orientation data were also recorded, as well as data quality indicators (beam echo and correlation magnitude) at each bin. The ADCP deployment configuration varied across sites based on factors such as water depth and expected currents (Kammerer et al. 2021). Either a Teledyne RD Instruments (TRDI) Workhorse Sentinel (300 kHz, 600 kHz, or 1200 kHz) or TRDI Long Ranger (75 kHz) was used. ADCPs were either bottom-deployed from a seabed-resting platform or moored from a taut line. As subsequently discussed, at some sites with relatively energetic currents, the latter configuration resulted in blow down angles exceeding the ADCP operational limits.

All ADCP data processing was conducted in MATLAB using custom scripts and functions. Raw survey data was provided by NOAA CO-OPS and QA/QC data using CO-OPS protocols were available through the CO-OPS web portal (C-MIST, cmist.noaa.gov). Raw data was converted from the proprietary Teledyne format to MATLAB format using the 'rdradcp' package (eoas.ubc.ca/~rich). Data were screened using the following criteria and time series points were excluded from further analysis if:

1. The bin was located above the free surface, based on the integrated depth sensor;
2. The correlation threshold for a particular combination of bin and time was below 64 counts or echo intensity was below 20 counts (Kammerer et al. 2021);
3. The instrument tilt exceeded 20°, which exceeds ADCP bin mapping limits (Mantovanelli et al. 2014), in which case all bins were discarded for that time; or
4. The combination of bin and time was contaminated by side lobe reflection from the free surface (Lentz et al. 2022).

Further details of the tilt calculation and side lobe threshold identification are given in Calandra et al. (2023). Of these criteria, the tilt thresholding and side lobe removal are distinct from standard CO-OPS quality assurance procedures (Kammerer et al. 2021) and resulted in the elimination of some data that

passed CO-OPS QA/QC. This is important for turbines deployed near the surface, since side lobe contamination artificially depresses measured current speeds (Letnz et al. 2022).

Following these steps, data were re-referenced to the water surface (i.e., placed into the same frame of reference as a floating turbine). The procedure and comparison to the CO-OPS data product is shown schematically in Figure 2 for a representative snapshot from the most energetic site identified in the re-analysis.

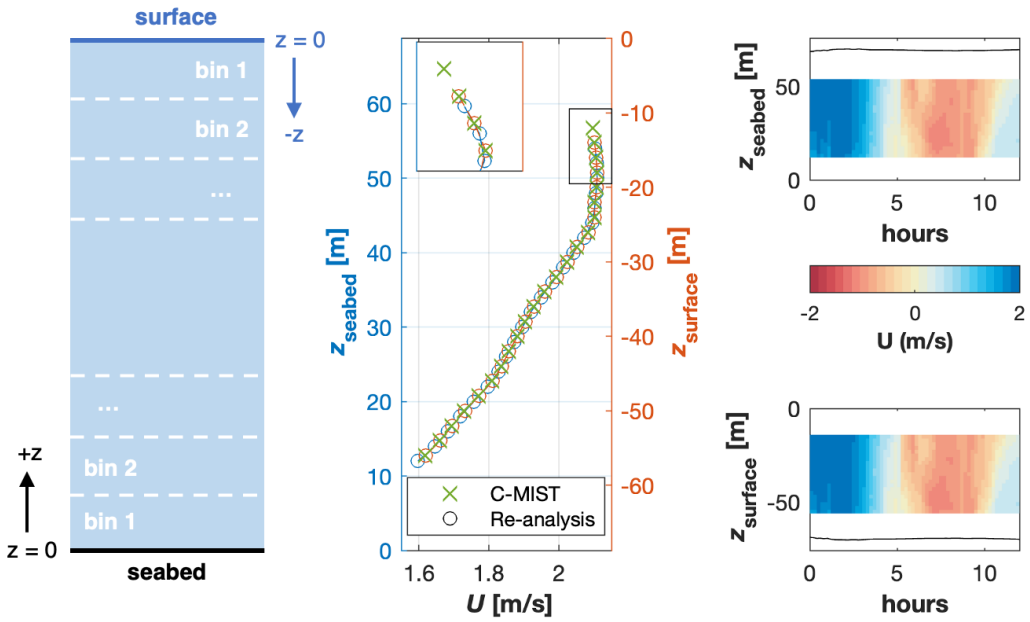

Figure 2: Seabed and surface-reference velocity profile comparison. (left) Coordinate transformation reference frames. (middle) Instantaneous velocity profiles at one representative time step for Site 32, with inset showing details for the upper profile. (right) Representative velocity time series for seabed- and surface-referenced profiles following QA procedures. Solid black lines represent the time-varying water surface or seabed elevation. The distances from the free surface and from the seabed are represented by $z_{surface}$ and z_{seabed}, respectively. (Calandra et al. 2023)

Model results of water level, velocity and turbulence parameters are automatically outputted in NetCDF format and no post-processing is required. Additional quantities derived from the model results (e.g., vorticity) are processed using either MATLAB or Python scripts and stored in NetCDF format. For model validation, model results are interpolated at the same water depth of ADCP data. Because the model uses sigma-stretch coordinate, variation of sea surface and total water depth are automatically accounted for.

6.5.3 Data Analysis

For ADCP data, turbine-independent calculations are first performed. For sites with measurement data that were of interest to Orbital Marine Power, the following plots were generated:

- Probability distributions of current speed and power density at depths corresponding to 25%, 50%, and 75% of the water column (three, superimposed lines). Current speed is discretized in 0.1 m/s increments and power density is discretized in 0.1 kW/m^2 increments.

- Mean and standard deviation of current direction as a function of depth, separated for ebb and flood tides.
- Time-average directional asymmetry (difference between flood and ebb, relative to an ideal offset of 180 degrees) as a function of depth.

In addition, the suitability of a log law representation of the vertical profile was considered for each site.

For turbine-dependent quantities, current time series are interpolated to the hub height of a hypothetical O2 turbine. Because it is economically desirable to deploy the largest possible turbine diameter for a given site, the size of candidate turbines varies across possible deployment sites, as summarized in Table 2. Hub height, z_{hub}, relative to the surface is given as

$$z_{hub} = D/2 + z_{clearance}$$

where D is the rotor diameter and $z_{clearance}$ is the tip clearance below the surface (3 m). The rotor diameter is determined based on the minimum water depth in the measurement time series from the ADCP pressure sensor, corrected for known stand-off distance between the pressure sensor and seabed. If the minimum water depth at a site is less than 29 m, the site is considered unsuitable for O2 deployment.

In some cases, valid data does not encompass hub height. In these cases, currents are extrapolated to hub height using a tangent profile, demonstrated to be robust to outliers (Calandra et al. 2023).

Table 2: Turbine diameter as a function of minimum water depth

Minimum water depth [m]	Turbine diameter [m]
29	18
31	20
33	22
35	24
37	26
39	28
41	30

Based on the hub-height time series of currents, the following turbine-dependent quantities were calculated:

- Probability distributions of current speed and power density in the same increments as turbine-independent quantities; and
- Time-average current speed and power density.

Since model results are output at normalized vertical layers and water depth changes over a tidal cycle, model results are interpolated to the hub-height, similar to the approach of ADCP data. For model data, analysis is conducted similar to the ADCP for model-data comparison. Additional analysis is carried out to identify high gradients, both horizontally and vertically, using spatial maps of technology-independent quantities.

7 PROJECT OUTCOMES

7.1 RESULTS

7.1.1 ADCP Measurements

ADCP data encompassed 46 locations in the San Juan Islands, as shown in Figure 3.

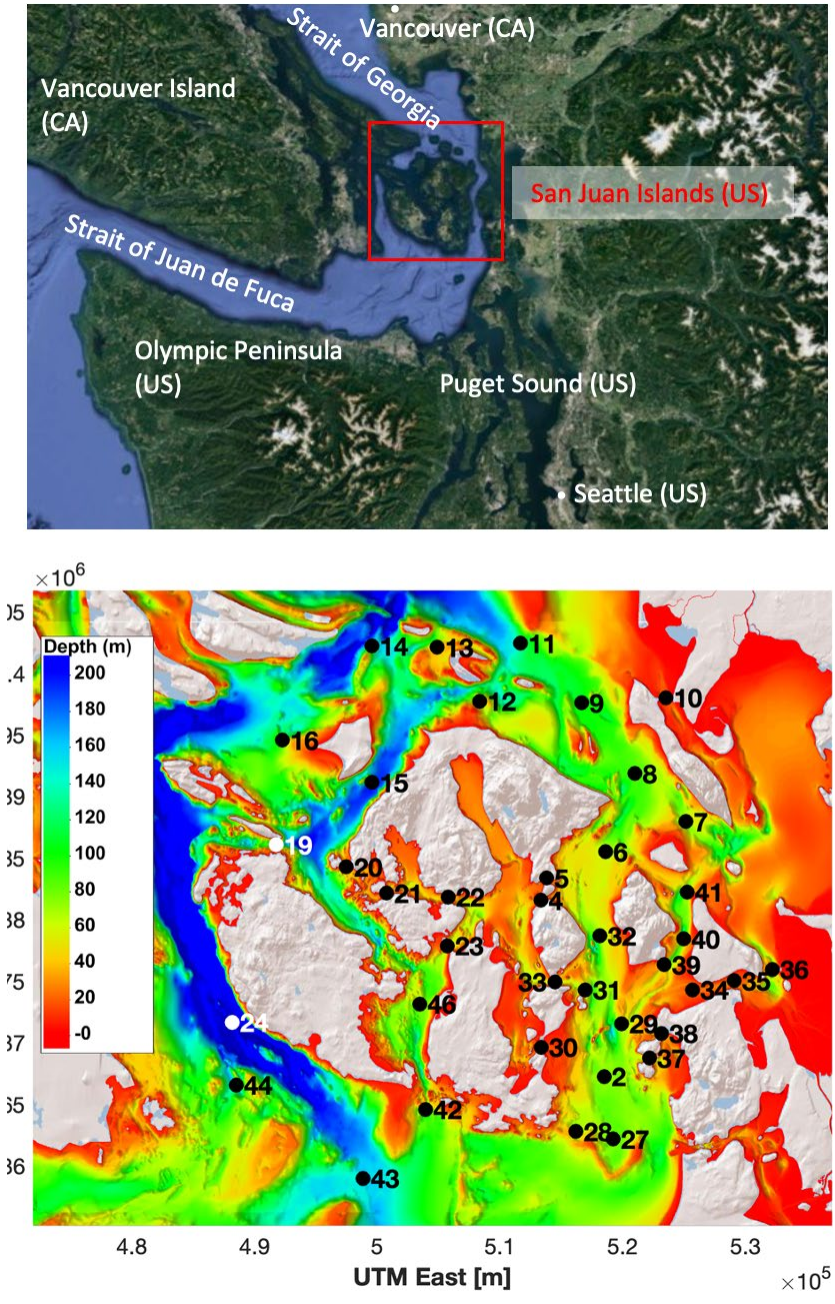

Figure 3: (top) Salish Sea geography with the San Juan archipelago outlined (source: Google Earth satellite imagery). (bottom) Bathymetric rendering of the San Juan archipelago with measurement sites numbered by

NOS designation. Not shown are sites without any valid current data (Site 1, located east of Site 27; Site 3 located north of Site 42; Sites 17 and 18, located at the western margin of Haro Strait).

Site characteristics are summarized in Table 3. The majority of surveyed sites had relatively low hub-height power density, with only three sites exceeding a threshold of 1 kW/m^2. Orbital Marine Power's initial screening had identified four locations of particular interest:

- Spieden Channel: NOS Site 19 is the closest station and had acceptable data quality;
- Western margin of Rosario Strait: NOS Site 32 is the closest station and had acceptable data quality;
- San Juan Channel: This channel lies south and west of NOS Sites 20 and 21, but was not surveyed; and
- Cattle Pass: This channel lies north of NOS site 42, but even at this location, where currents are weaker than in the pass itself, turbine-dependent quantities could not be calculated because mooring blowdown resulted in a limited set of depths with valid data. The measurement site within Cattle Pass (NOS Site 3) yielded no valid data.

The remainder of the measurement results focus on NOS Sites 19 (Spieden Channel) and 32 (western margin of Rosario Strait).

Table 3: Site summary information ordered by power density. Entries in bold correspond to locations of particular interest to Orbital Marine Power based on initial screening. Speed and power density are time averaged quantities at hub height.

Site Number	Latitude [deg]	Longitude [deg]	Duration [days]	Water Depth [m]	Turbine Diameter [m]	Speed [m/s]	Power Density [kW/m^2]	Note
40	48.5585	-122.6618	61	75	30	0.96	1.20	
32	**48.5610**	**-122.7543**	**63**	**69**	**30**	**0.93**	**1.15**	
39	48.5396	-122.6834	63	45	30	0.93	1.02	
24	48.4980	-123.1599	130	306	30	0.74	0.88	b
19	**48.6278**	**-123.1117**	**53**	**119**	**30**	**0.87**	**0.81**	**b**
29	48.4968	-122.7308	64	59	30	0.80	0.71	
41	48.5928	-122.6577	64	72	30	0.78	0.66	
42	48.4344	-122.9466	67	122	30	0.78	0.65	b
2	48.4581	-122.7501	125	71	30	0.73	0.59	
6	48.6224	-122.7476	127	65	30	0.73	0.55	b
44	48.4521	-123.1554	69	144	30	0.70	0.48	b
28	48.4181	-122.7812	60	70	30	0.69	0.48	
14	48.7731	-123.0058	56	131	30	0.71	0.43	b
38	48.4895	-122.6867	66	34	20	0.68	0.36	
37	48.4716	-122.6998	67	37	22	0.56	0.25	
15	48.6734	-123.0060	53	200	30	0.57	0.25	b
8	48.6794	-122.7147	123	88	30	0.55	0.24	b
27	48.4125	-122.7403	60	82	30	0.51	0.24	
13	48.7721	-122.9337	54	37	22	0.57	0.22	

31	48.5216	-122.7707	64	51	30	0.49	0.15	
12	48.7326	-122.8864	54	69	30	0.47	0.14	
23	48.5538	-122.9226	54	52	30	0.48	0.13	
46	48.5114	-122.9529	68	74	30	0.49	0.13	
9	48.7313	-122.7734	55	102	30	0.44	0.13	
16	48.7042	-123.1048	56	65	30	0.47	0.12	
33	48.5274	-122.8040	64	61	30	0.38	0.10	
43	48.3840	-123.0157	69	155	30	0.40	0.08	b
22	48.5897	-122.9217	57	34	20	0.37	0.05	
20	48.6115	-123.0341	54	38	24	0.38	0.05	
11	48.7749	-122.8410	56	127	30	0.34	0.05	b
26	48.9389	-123.1651	57	119	30	0.34	0.04	
7	48.6442	-122.6587	51	73	30	0.26	0.02	
36	48.5359	-122.5639	66	83	30	0.27	0.02	
4	48.5871	-122.8193	57	18				a
5	48.6033	-122.8127	56	20				a
10	48.7349	-122.6802	51	19				a
21	48.5925	-122.9896	54	28				a
25	48.8338	-122.7279	58	20				a
30	48.4797	-122.8189	66	25				a
34	48.5212	-122.6522	65	20				a
35	48.5277	-122.6060	65	20				a
1	48.4062	-122.6431	135	36				c
3	48.4610	-122.9520	80	137				c
17	48.6912	-123.2450	57	227				c
18	48.5887	-123.2258	57	264				c
45	48.5567	-122.9985	67	160				d

Notes:
a: Insufficient water depth to deploy a turbine
b: No data at hub height – currents extrapolated to hub height using tangent profile
c: No depth bins passed QA/QC thresholds
d: Insufficient valid data to extrapolate to hub height

7.1.2 Turbine-Independent Quantities

Figure 4 shows the probability distributions of current speed and power density for up to three positions in the water column at each site. Neither site has significant variations in the velocity distribution with depth, indicating a relatively blunt velocity profile. Both sites have speed distributions that are skewed low as a consequence of the diurnal inequality (two ebb and flood tides of unequal strength in a single lunar day) present throughout Salish Sea. This skewness is magnified in the power density distribution due to the cubic dependence of power on speed.

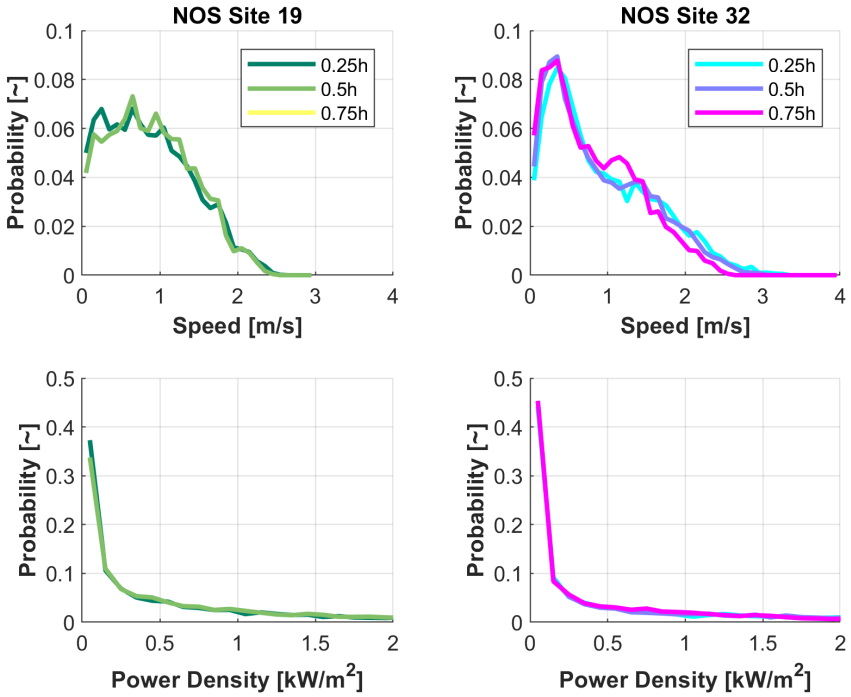

Figure 4: Probability distributions of speed and power density for NOS Site 19 (Spieden Channel) and 32 (Rosario Strait). H corresponds to time-average water depth and distributions are referenced to the surface (e.g., 0.25h corresponds to a depth at the upper quarter of the water column). ADCP data are not available for 0.75h at NOS Site 19.

Figure 5 summarizes directional variations within ebb and flood cycles with depth, as well as the degree of asymmetry in the current direction relative to bi-directional currents in which ebb and flood are opposed by exactly 180 degrees. For both sites, the direction of ebb and flood are relatively consistent with depth with no more than 20 degrees of variation relative the mean direction at any depth. Currents are nearly bidirectional at NOS Site 32 (Rosario Strait), but are less aligned, particularly at depth, at NOS Site 19 (Spieden Channel).

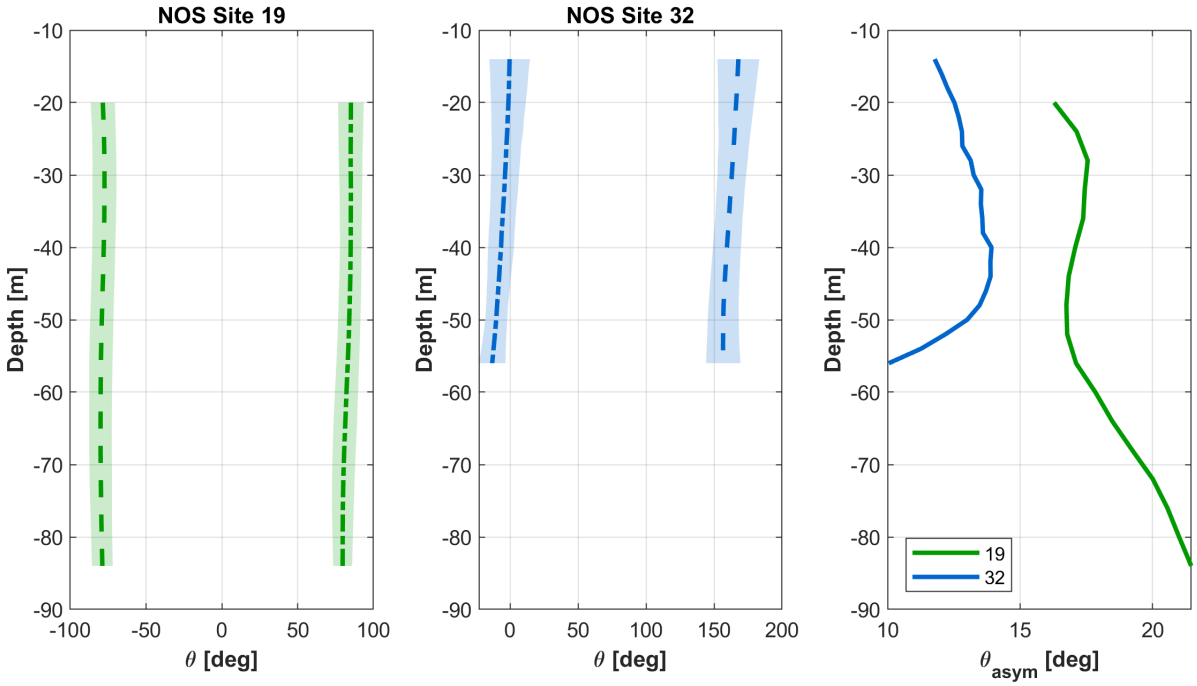

Figure 5: Mean flood (positive) and ebb (negative) directions (dashed lines) and variation (shading) with depth for NOS Sites 19 (Spieden Channel) and 32 (Rosario Strait), as well as directional asymmetry relative to bi-directional currents (180 degrees out of phase).

A summary of the log law fit is shown in Figure 5. At Site 19, on ebb, surface roughness is physically plausible (< 10 mm) and R^2 values suggest that the profile is relatively well described by a log law. In contrast, while the surface roughness remains plausible on flood, the R^2 values are negative, meaning that the log law profile fails to describe the vertical profile. At Site 32, on ebb, surface roughness is non-physically large, even though R^2 values suggest a good fit. Recall that surface roughness is a parameterization of the friction associated with the seabed – it is not indicative of the actual size of the seabed pavement. On flood, surface roughness is plausible and R^2 values are moderate. The relatively poor descriptive power of the log law fit and non-physical surface roughness values may be a consequence of bathymetric influences on the channel boundary layer.

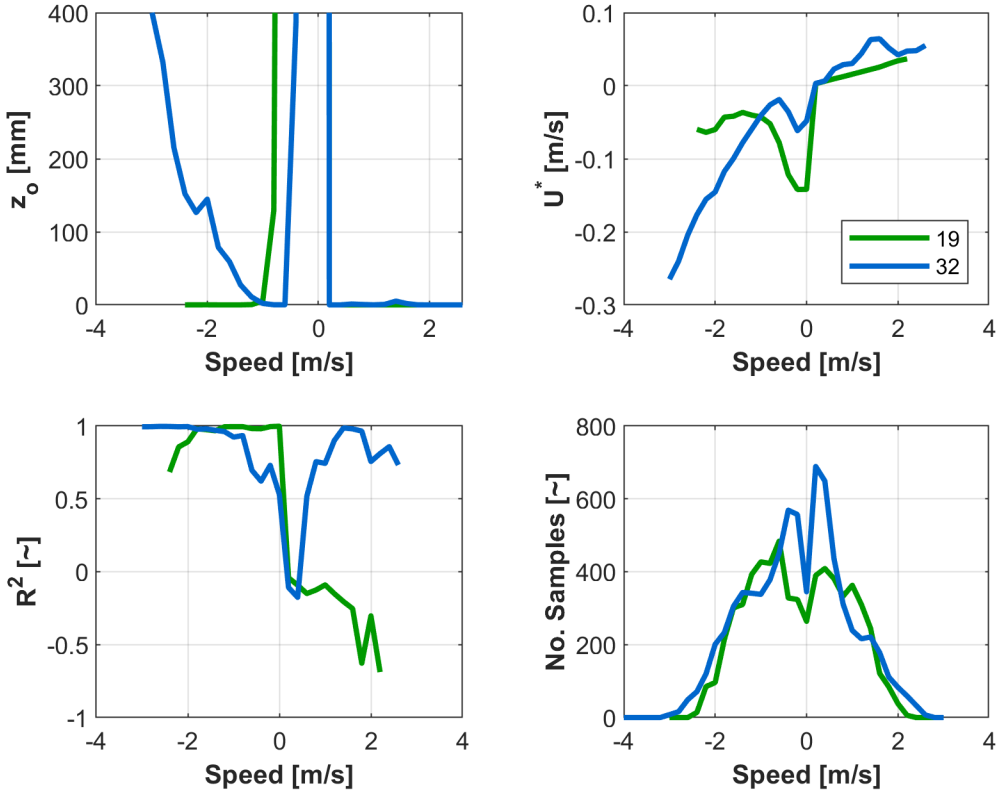

Figure 6: Log-law fit statistics for NOS Site 19 (Spieden Channel) and 32 (Rosario Strait). Y-axis for surface roughness is truncated for clarity.

7.1.3 Turbine-Dependent Quantities

Hub-height probability distributions of current speed and power density are shown in Figure 4. NOS Site 32 has a substantially higher time-average power density (Table 3) owing to the longer tail to the current speed distribution.

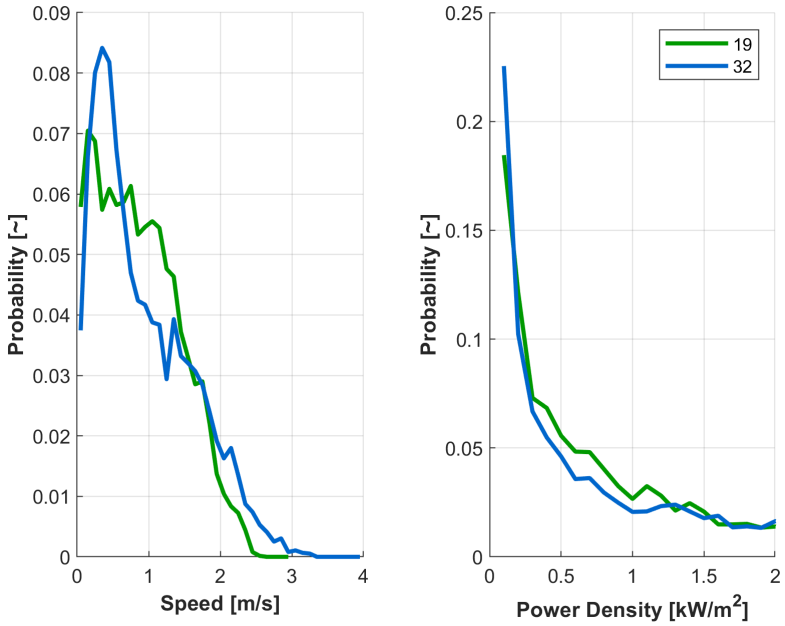

Figure 7: Probability distributions of hub-height speed and power density for NOS Site 19 (Spieden Channel) and 32 (Rosario Strait).

7.1.4 Model-Measurement Comparison

We consider model-measurement agreement for current speed and power density for four of the most energetic sites. Power density is a particularly sensitive comparison metric because relatively small errors in current speed are substantially magnified and can be significant for turbine power generation. As shown in Figure 7, model and measurements are in better agreement for time-average speed than time-average power density. While model-measurement speed comparisons are quite good for NOS Sites 32 and 39, power density still diverges between model and measurement at these locations, albeit to a lesser extent than for Sites 19 and 40. Given the small sample size (i.e., four sites), we do not infer general over- or under-prediction of modeled power density relative to measurements. Rather, we note that these discrepancies place limits on interpreting true variations in power generation potential within the San Juan Islands. Further, we emphasize that this is a numerical model that has undergone significant grid refinement relative to prior work (Yang et al. 2021). As such, improving model-measurement agreement for power density would likely require bathymetric data with greater resolution and accuracy than the existing digital elevation model of Salish Sea.

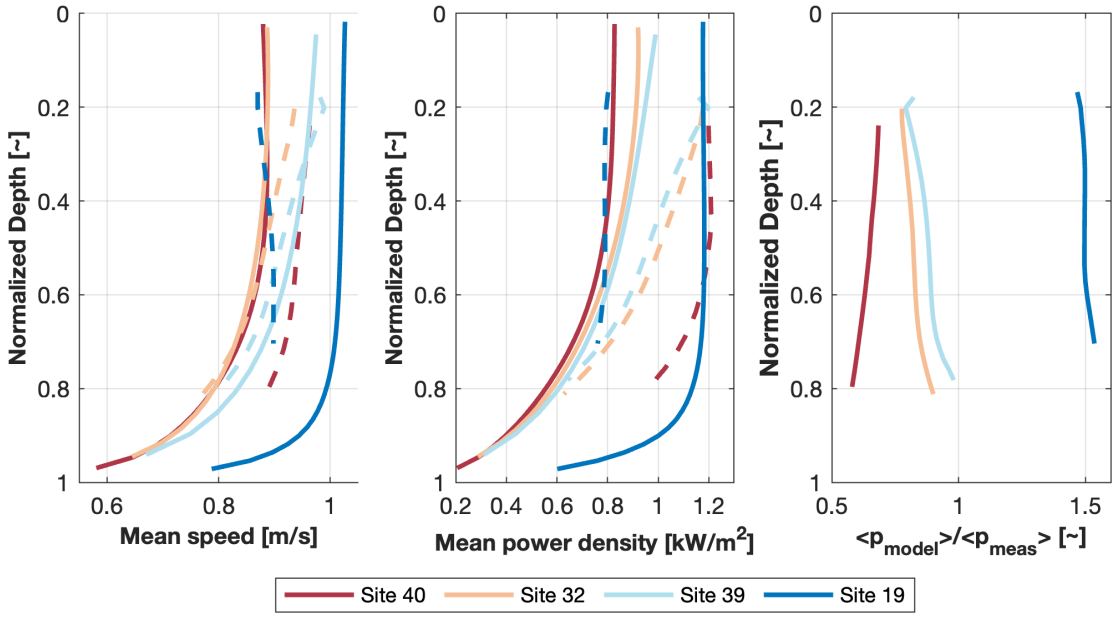

Figure 8: Comparison of model (solid line) and measurement (dashed line) speed (left) and power density (middle) profiles for four energetic sites. (right) Ratio of model and measurement power density profiles. To facilitate visual comparison across sites, depths are normalized by their time-average value.

7.1.5 Numerical Model Refinement

PNNL refined model grid for waterways around the San Juan islands. In most of the areas, the side length of the triangular grid cell was reduced by half so that the number of grid cells was quadrupled. For example, in Spieden Channel (**Figure 9**), the grid resolution (in terms of triangular side length) was now refined to ~50 meters, which substantially improves channel representation in the hydrodynamic model. In addition to lateral direction refinement, we increased model resolution in the vertical direction by doubling the number of sigma layers from 20 in the previous model configuration to 40 layers (**Figure 10**). To further improve model representation near the surface and bottom boundaries, a parabolic profile function was used to allow for higher vertical resolutions toward both boundaries.

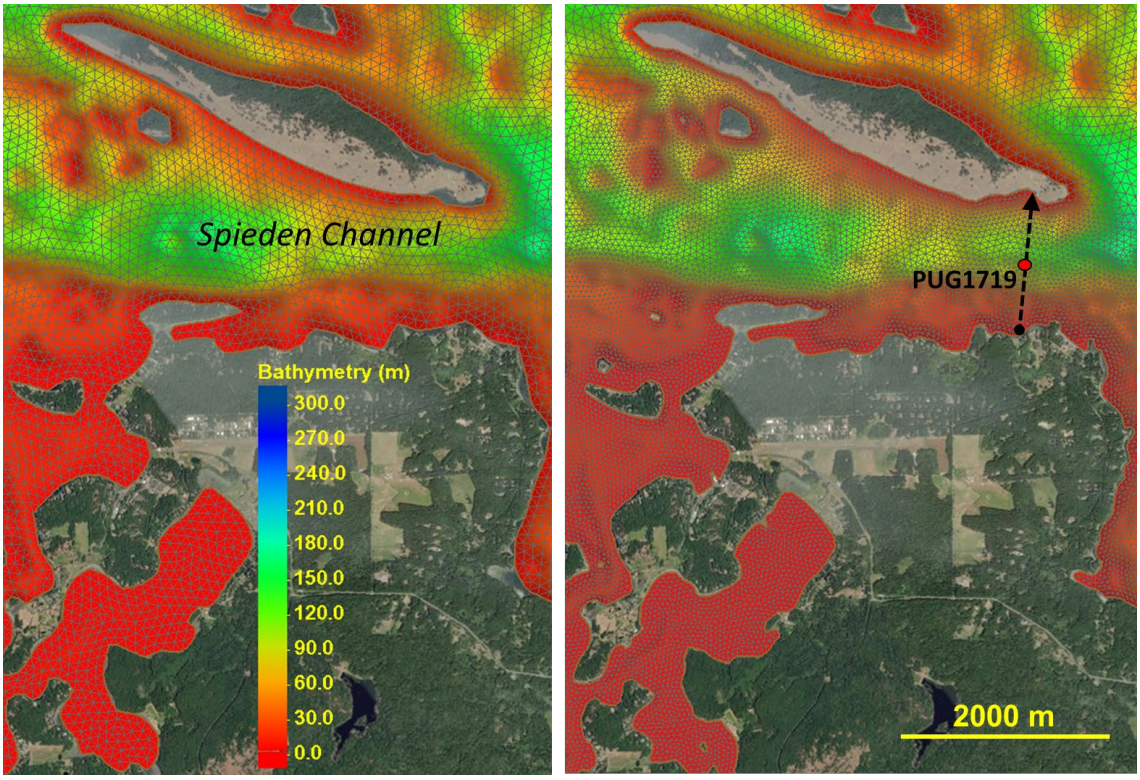

Figure 9: An example comparison of model grid resolution between the original (Yang et al., 2021) (left panel) and refined (right panel) models in the Spieden Channel region. The circular marker in the middle of channel denotes the location of NOS Site 19.

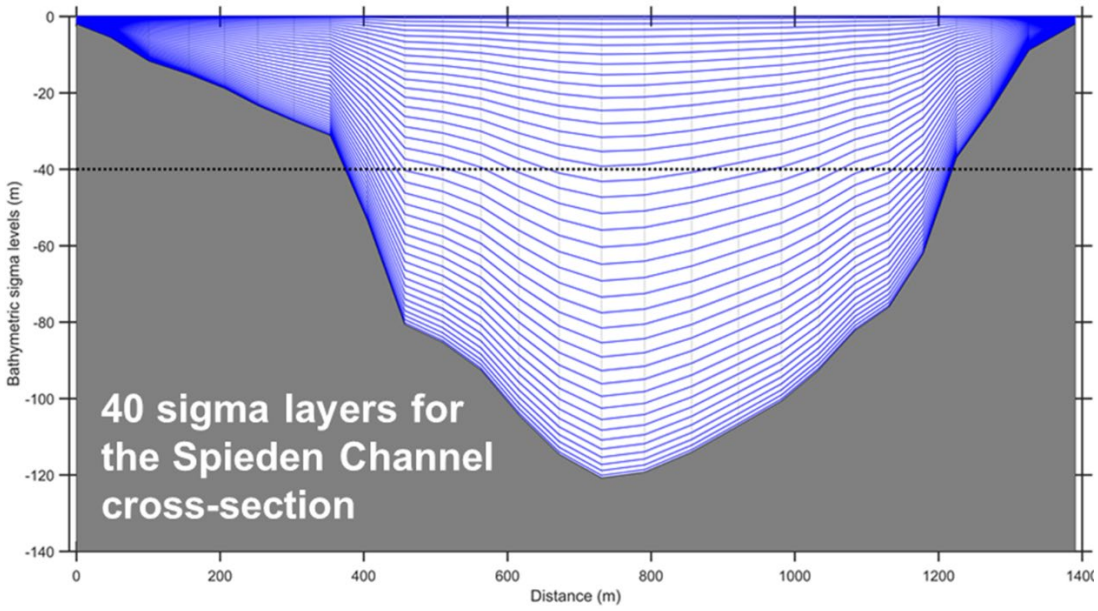

Figure 10: Sigma layer profiles along the Spieden Channel cross-section indicated in Figure 9.

The refined hydrodynamic model was subsequently validated by comparing water level and velocity model output against field observations at selected tidal gauges and velocity survey stations in the San Juan Archipelago to assure the refined model performed at a better or comparable level to the previous model in Yang et al. (2021). For these quantitative comparisons, 12-min, high-frequency model output was used. **Figure 11** shows example time series comparisons of model predicted surface water elevations against field observations at four representative tidal gauges in the Salish Sea. The results are comparable to those in the previous model. **Figure 12** and **Figure 13** show depth-averaged velocity comparisons between model predictions and field observations at two NOS current survey sites in the San Juan Archipelago. Model predictions matched field observations very well in terms of both magnitude and phase. Quantitative error statistics further confirmed the refined has a slightly better performance than the previous model, e.g., RMSE of 0.25 m/s vs. 0.26 m/s at PUG1732 and 0.21 m/s vs. 0.24 m/s at PUG1739.

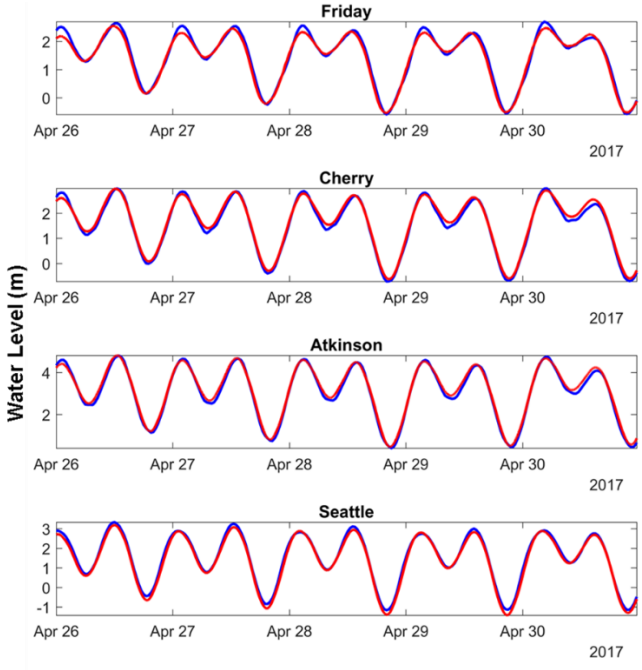

Figure 11: Example water level comparisons at four tidal gauges in the Salish Sea (from top to bottom: Friday Harbor, Cherry Point, Atkinson Point, and Seattle). The gauge locations can be found in Yang et al. (2021).

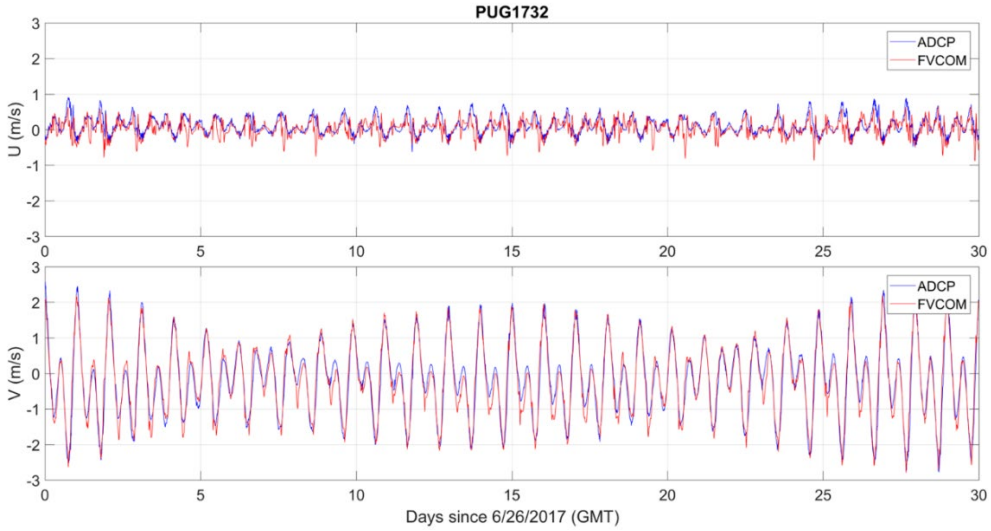

Figure 12: Example depth-averaged velocity comparisons at NOS current survey station PUG1732 (top panel: east velocity; bottom panel: north velocity).

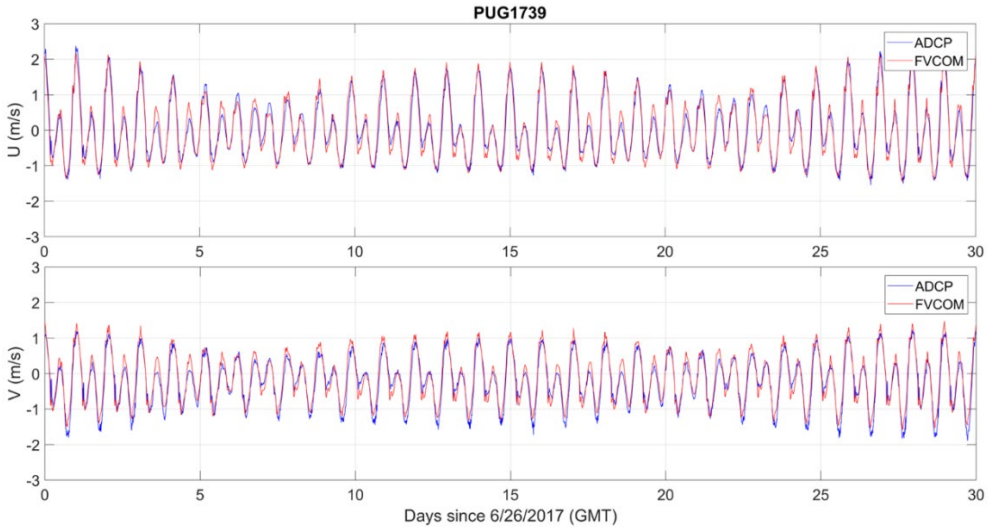

Figure 13: Example depth-averaged velocity comparisons at NOS current survey station PUG1739 (top panel: east velocity; bottom panel: north velocity).

7.1.6 Simulated 2-D Hydrodynamic Properties

In addition to the high-frequency station output that was used for model-data comparisons at NOS survey sites in the previous sections, the hourly, domain-wide model output was processed to assess the spatial distributions of major hydrodynamic properties around the San Juan Islands. **Figure 14** and **Figure 15** show the depth-averaged, 2-D velocity field during the peak flood and ebb tides, respectively. Strong tidal currents exceeding 3 m/s can be seen at places. **Figure 16** and **Figure 17** show the corresponding turbulent kinetic energy (TKE) distributions, which again exhibit strong spatial gradients of turbulence across the model domain. For instance, the Cattle Pass area shows persistently high TKE during both

peak flood and ebb tides, which is also consistent with existing knowledge of that area. **Figure 18** and **Figure 19** show the depth-averaged vorticity field. Due to the presence of complex geometric features such as numerous headlands and meandering channels, high vorticities occur throughout the model domain.

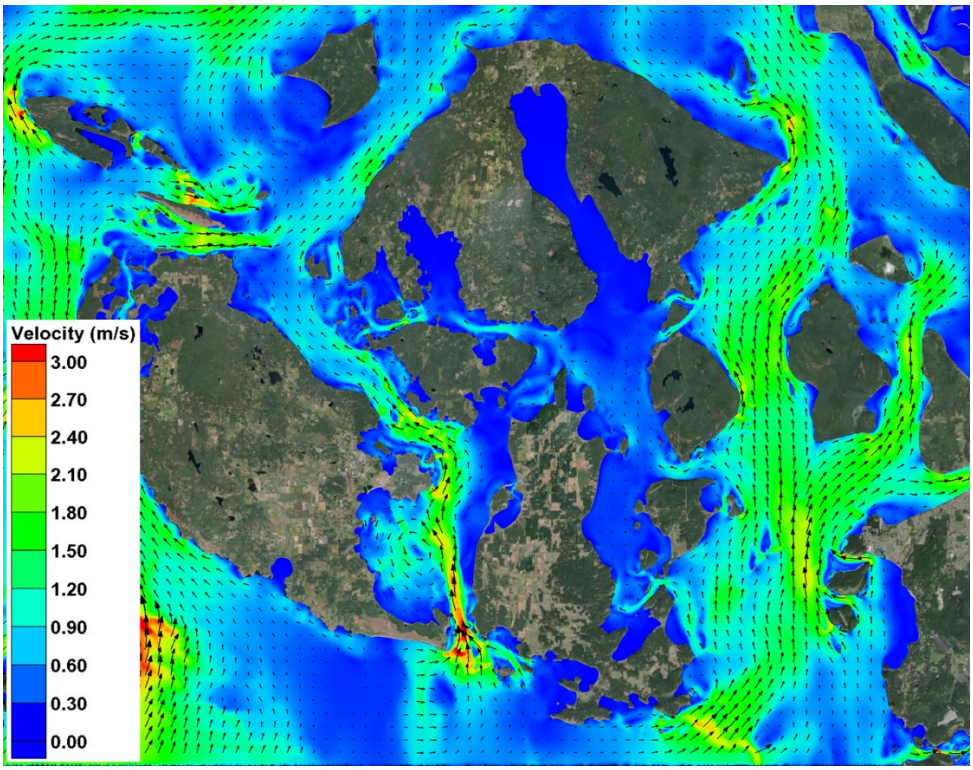

Figure 14: Snapshot of depth-averaged 2-D current field during the peak flood (2017-04-30 00:00:00 GMT).

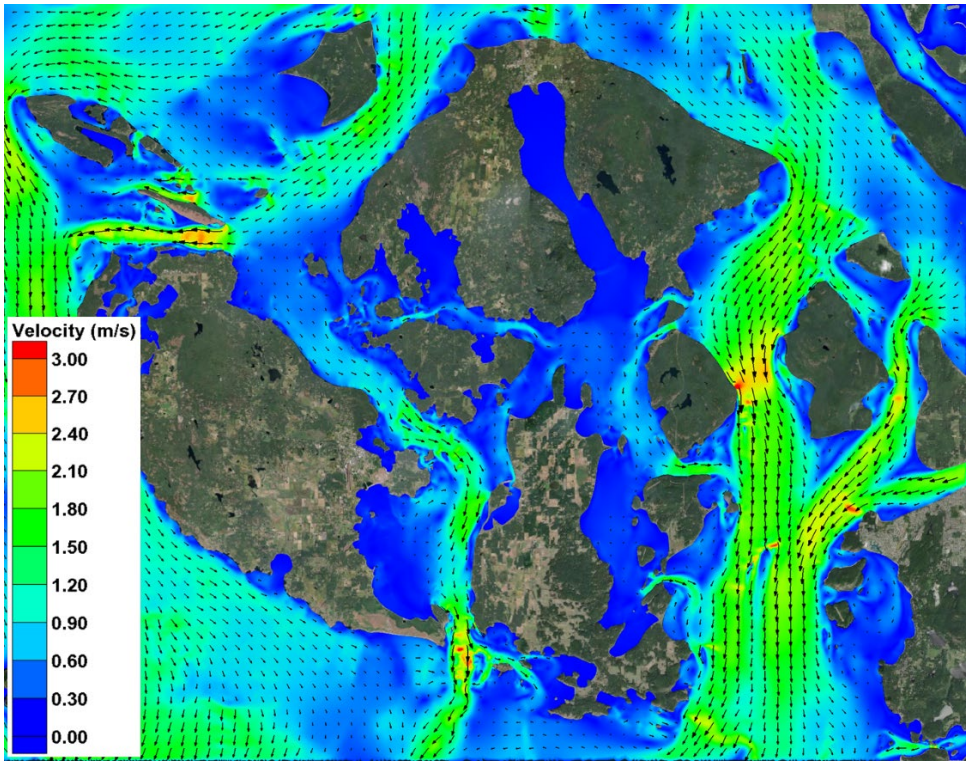

Figure 15: Snapshot of depth-averaged 2-D current field during the peak ebb (2017-04-30 19:00:00 GMT).

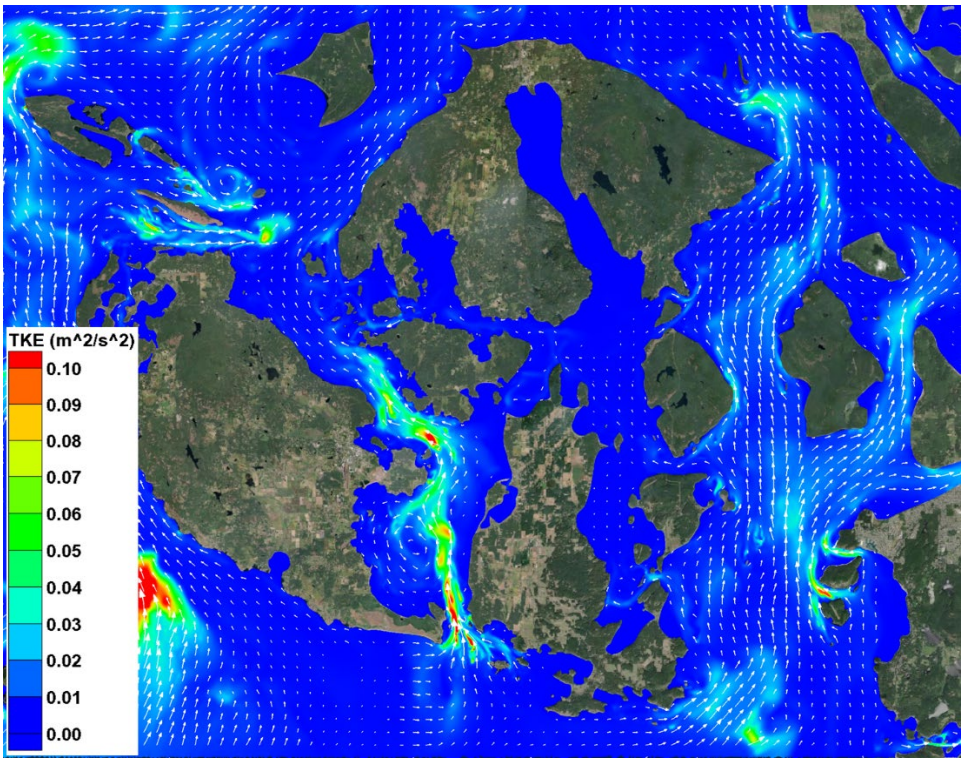

Figure 16: Snapshot of depth-averaged turbulent kinetic energy distribution during the peak ebb (2017-04-30 00:00:00 GMT).

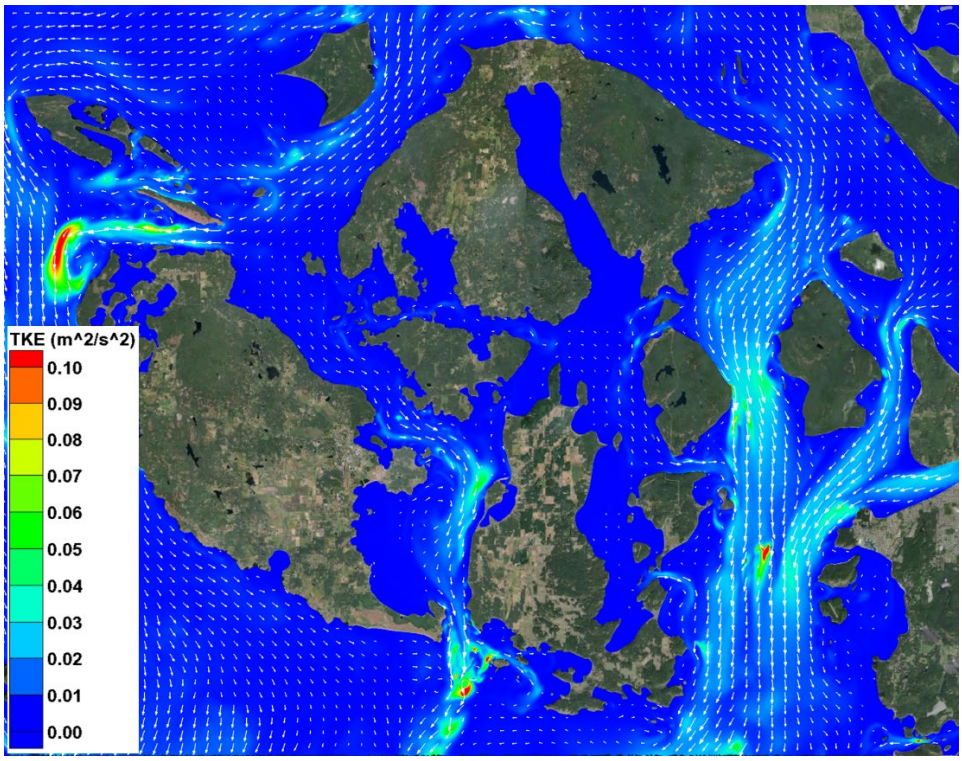

Figure 17: Snapshot of depth-averaged turbulent kinetic energy distribution during the peak flood (2017-04-30 19:00:00 GMT).

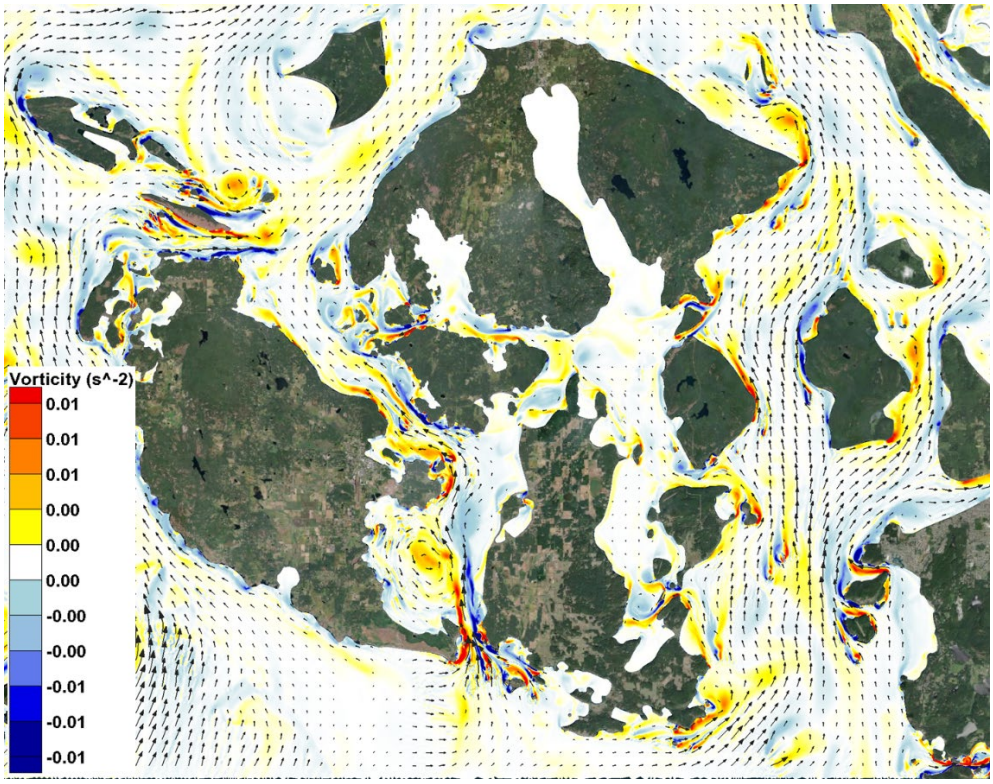

Figure 18: Snapshot of depth-averaged vorticity field during the peak flood (2017-04-30 00:00:00 GMT).

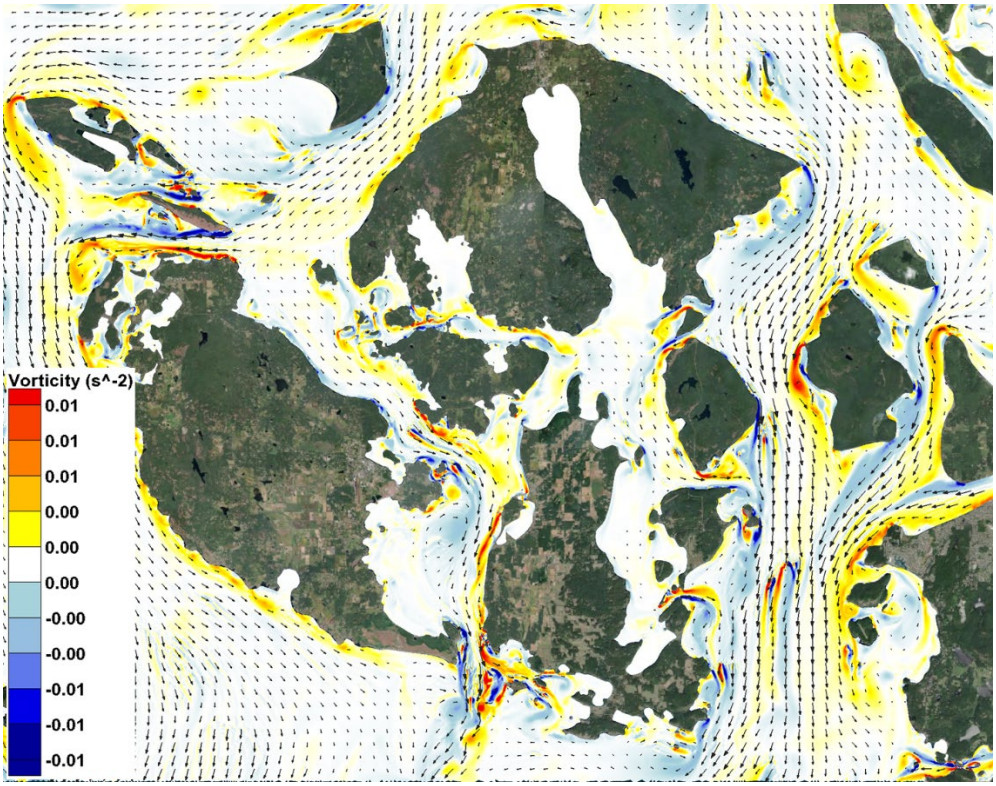

Figure 19: Snapshot of depth-averaged vorticity field during the peak ebb (2017-04-30 19:00:00 GMT).

7.1.7 Power Density Distributions

Depth-averaged power density were calculated based on model predicted 4-D velocity field. **Figure 20** and **Figure 21** show the instantaneous power density distributions during peak ebb and flood tides. High instantaneous power density exceeding 10 kW/m^2 can be seen in several tidal channels. **Figure 22** shows the time- and depth-averaged power density distribution over the 2-month simulation period. Despite compared to instantaneous values, the averaged power density is considerable smaller, many areas appear to have abundant tidal power resources (e.g., power density > 1 kW/m^2). **Figure 23** shows the mean power density profile along one cross-section in the Rosario Strait. Power density shows strong spatial heterogeneity, e.g., power density increases toward the west side of the channel and the surface.

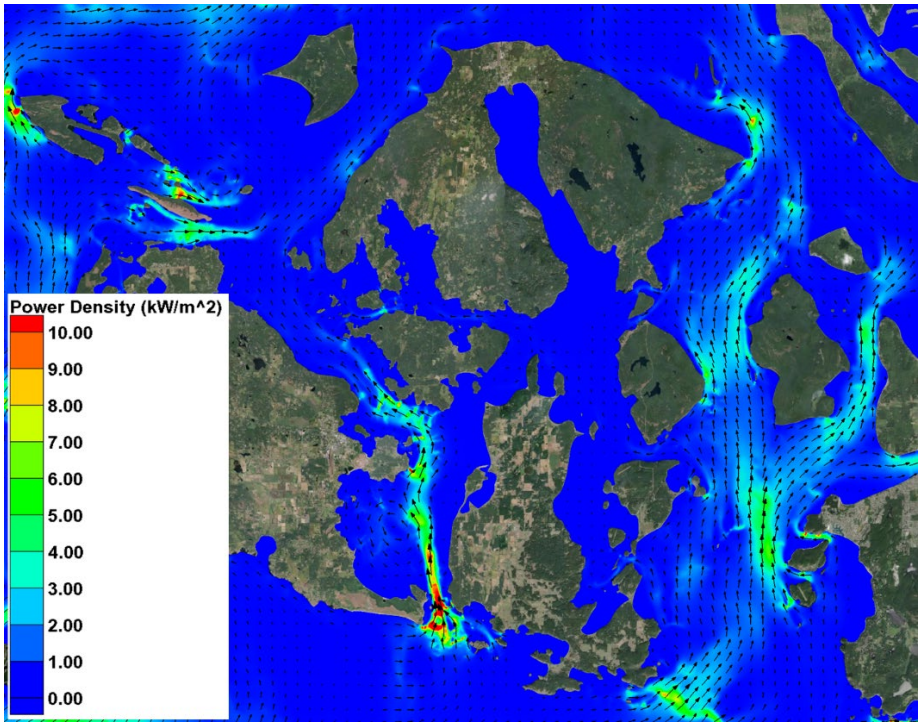

Figure 20: Snapshot of depth-averaged power density distribution during the peak flood (2017-04-30 00:00:00 GMT).

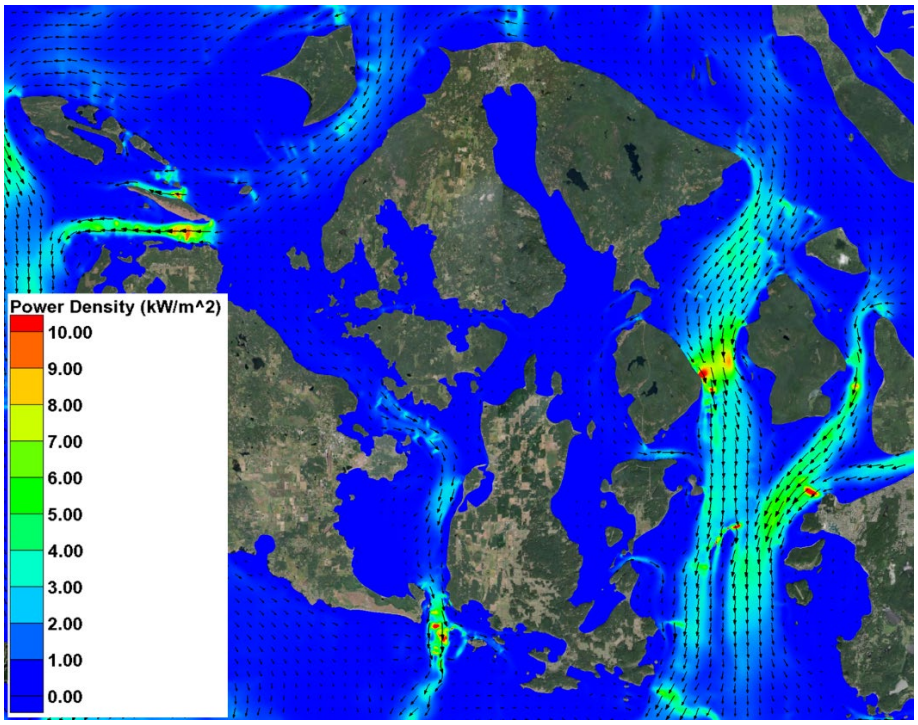

Figure 21: Snapshot of depth-averaged power density distribution during the peak ebb (2017-04-30 19:00:00 GMT).

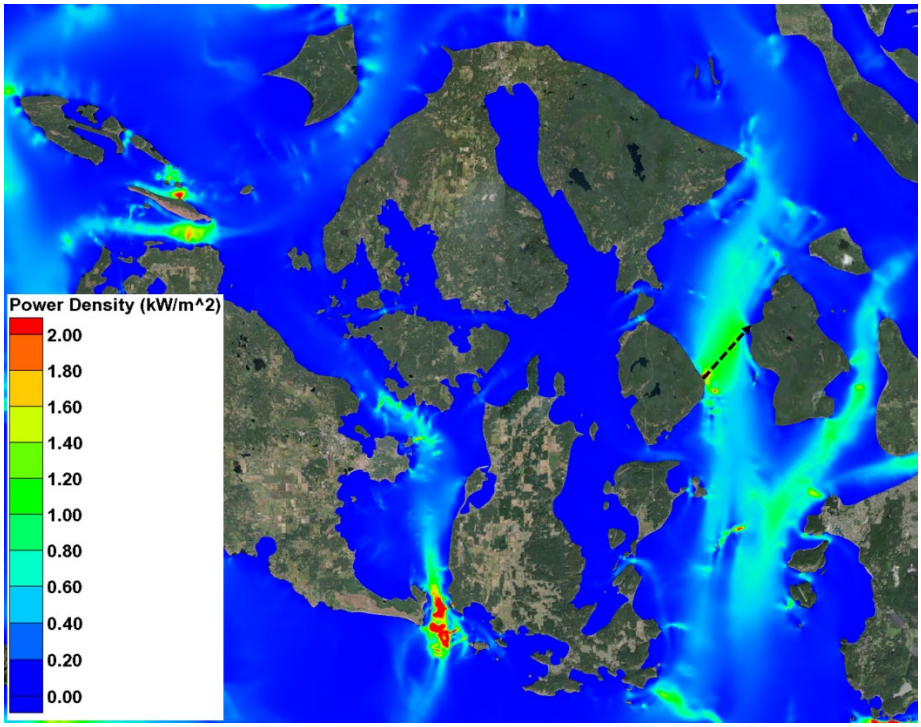

Figure 22: Time- and depth-averaged power density distribution over the two months of model simulation period.

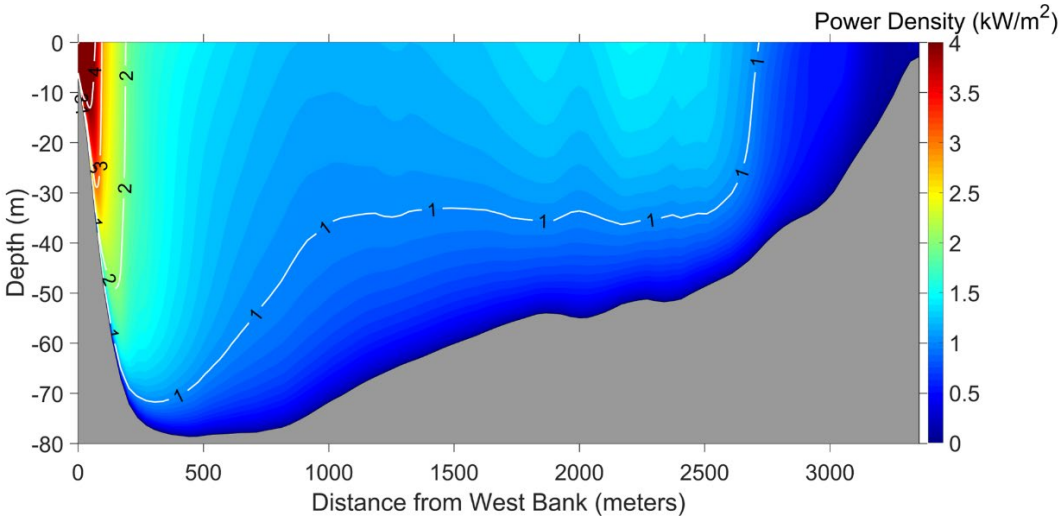

Figure 23: Cross-channel mean power density distribution over the two months of model simulation period. The cross-section is inside Rosario Strait and indicated in Figure 22.

7.1.8 AEP Calculation

Example AEP was calculated for a surface-deployed dual-rotor, horizontal axis tidal turbine based on typical turbine specifications, e.g., 15-m rotor radius, hub height 18 m below the surface, water-to-wire coefficient of 0.39, and rated at 2.4 MW. **Figure 24** shows the AEP spatial distributions for one section of the Rosario Strait between Blakely and Cypress Islands. High AEP close to 10 GWh/year is expected toward the west side of the channel (e.g., adjacent to Blakely Island) for a turbine deployed there. **Figure 24** further evaluated the turbine capacity factor (CF), a parameter reflecting the degree to which turbine generating capacity is utilized (i.e., ratio of average to rated power). The results suggest that a high CF near 0.5 is expected for turbines deployed toward the west side of the channel. Interestingly, NOS survey site does not necessarily fall in the high-velocity region, e.g., PUG1732 in **Figure 24**, justifying the importance of having a high-resolution hydrodynamic model to support tidal turbine siting.

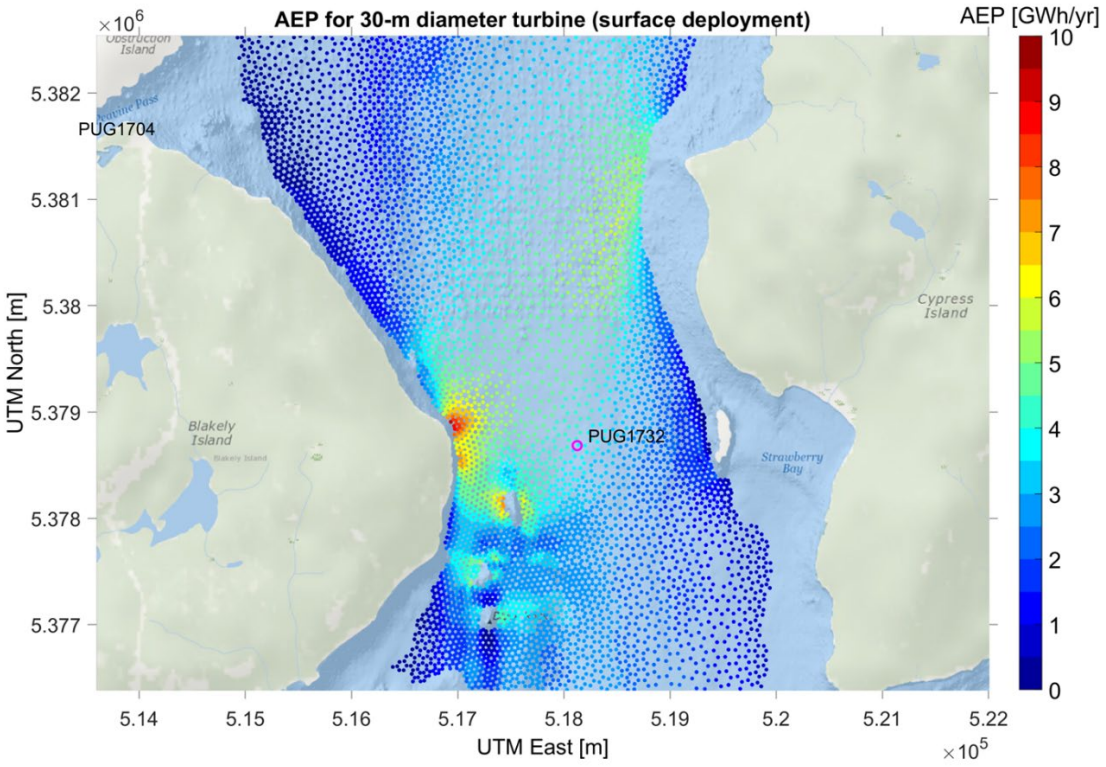

Figure 24: Example AEP estimations for surface-deployed turbines in Rosario Strait. Water depths shallower than 36 m are unable to accommodate the turbine rotor and excluded from the plot. The ''o'' symbols indicate the NOS current survey station PUG1732.

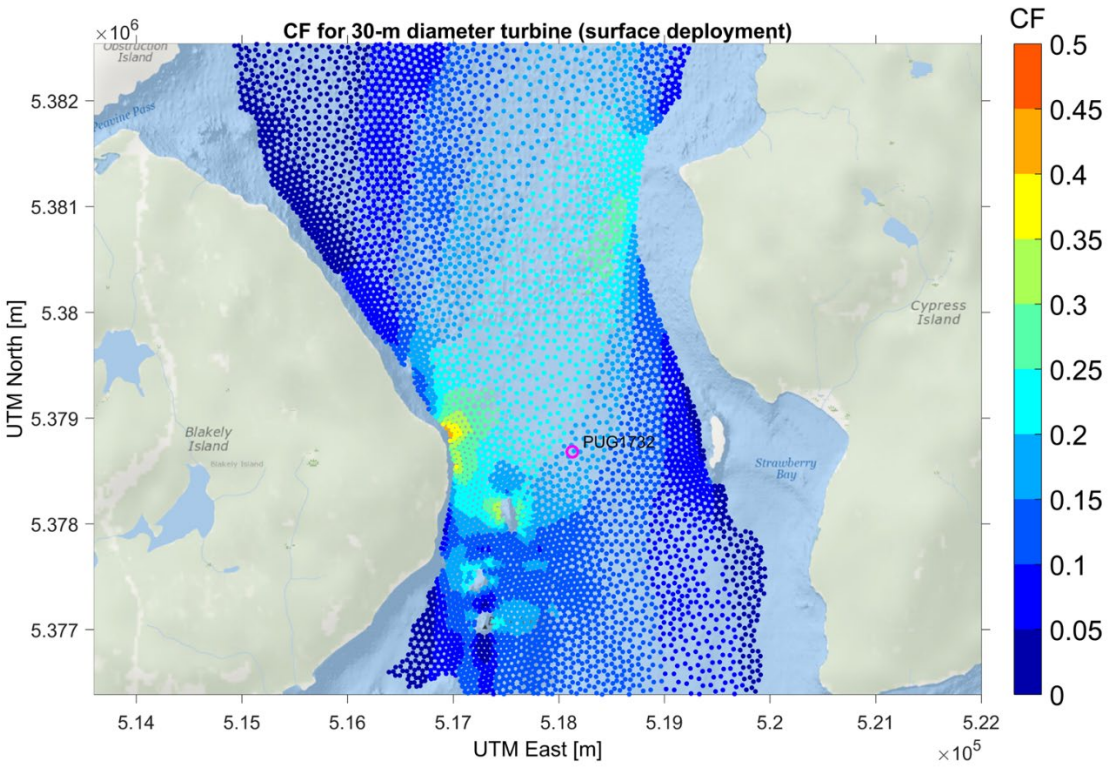

Figure 25: Example CF calculations for surface-deployed turbines in Rosario Strait. Water depths shallower than 36 m are unable to accommodate the turbine rotor and excluded from the plot. The "o" symbols indicate the NOS current survey station PUG1732.

7.2 Lesson Learned and Test Plan Deviation

Measurement Quality

Because the primary purpose of the NOS survey was to characterize tidal currents for navigation, the survey did not necessarily target locations with the strongest currents. In addition, at a number of locations with strong currents (e.g., Cattle Pass), the taut-line moorings experienced significant "blow down" with ADCP tilt angle routinely exceeding the QA threshold. We note that taut-line moorings can be used for tidal current resource characterization (e.g., StableMoors in Harding et al. 2017), but these differ from the standard NOS hardware.

Vertica Profile Fits

At project initiation, it was assumed that calculating best fit regressions of the vertical profile to a log law could provide additional insight into site characteristics. Specifically, the values of surface roughness derived from measurements could potentially be compared to roughness values employed in

simulation. Unfortunately, at sites of interest, the log law proved to be an unhelpful descriptor of the vertical profile. During some stages of the tide, plausible roughness values were obtained, but the resulting analytical profile did not match the observed profile (i.e., low R^2 values). During others, the derived surface roughness was implausibly large. These disagreements may be a consequence of the complicated bathymetry within the San Juan Islands, which causes the vertical profile to depart from a classical log law. Because of this, Calandra et al. (2023) explored several possible vertical profiles and determined that empirical tangent fits were the least likely to produce non-physical outliers.

Rotor-Averaged versus Hub-Height Quantities

At project initiation, we expected that the most accurate technology-dependent quantities would be derived from a spatial average over the rotor swept area. For measurements, we found this to be problematic because of the extent of available data. Specifically, because of side lobe contamination, there were no locations where valid velocity profiles extended over the entire rotor swept area. Because of this, velocities higher in the water column would require extrapolation based on a profile fit to data. Calandra et al. (2023) contrasted AEP from hub-height power density to a rotor average for a turbine at mid-water and found relatively low deviations (< 3%) for energetic sites. These deviations were of similar magnitude to the deviations in rotor-averaged power density when different fits (power law, log law, tangent, linear) were used to extrapolate from available data. Because of this, hub height quantities were used throughout this report and are likely adequate in most situations.

Extrapolation of Current Direction

We had originally anticipated calculating directional quantities at hub height comparable to turbine-independent metrics (e.g., current direction, asymmetry). However, this proved problematic because of the number of locations where current measurements at hub height were not available. While we were able to demonstrate the effectiveness of a simple tangent extrapolation for speed in Calandra et al. (2023), it is less clear whether that method would be appropriate for extrapolating current direction. Because the mooring system allows the O2 turbine to passively yaw with moderate variation in current direction, we did not pursue this further.

Model Accuracy

Because the numerical model for the study region had gone through substantial validation against current speeds and surface elevation (Yang et al. 2021), we anticipated that model-measurement agreement would be quite good throughout the domain. However, when compared on the basis of power density, which is sensitive to relatively small errors in current speed, models and measurements disagreed substantially at several sites. While there is insufficient measurement data available at energetic sites to draw global conclusions about model accuracy, this suggests that increasing model accuracy would likely require more accurate and higher resolution bathymetric data for the region.

- One of the most important factors that affects the model accuracy is bathymetry. Model bathymetry is based on an old bathymetry dataset released in 2014. Therefore, one potential improvement of model accuracy is to obtain more accurate bathy data and refine the model bathymetry.

8 CONCLUSIONS AND RECOMMENDATIONS

The project team conducted an evaluation of tidal current resources in the San Juan Islands using a combination of measurement re-analysis and numerical simulation. These data were used by Orbital Marine Power to estimate AEP. The results indicate that multiple locations in the region have appreciable currents that could be harnessed for tidal power generation.

Neither models nor measurements paint a complete picture of the tidal power potential. While the NOS measurement campaign distributed a relatively large number of ADCPs (46 sites total) only a handful of these produced data of acceptable quality in locations with high currents. In several cases, locations with high currents caused mooring motion (e.g., blow down) that rendered the data unusable for this analysis. In contrast, the numerical model produced a comprehensive spatial and temporal description of currents throughout the region. However, comparisons of power density between model and measurement at energetic locations revealed unexpectedly large disagreements, potentially associated with the quality of the available bathymetric data. This suggests that, should further site development activities be conducted in the San Juan Islands, resource characterization should continue to involve a combination of modeling and measurements.

9 REFERENCES

Calandra, G., Wang, T., Miller, C., Yang, Z., and Polagye, B. (2023) A comparison of the power potential for surface- and seabed-deployed tidal turbines in the San Juan archipelago, Salish Sea, WA. *Renewable Energy*. 214. doi: 10.1016/j.renene.2023.05.099.

Enders, L., Guerra, M., Karsten, R., Culina, J., Locke, J., and Hay, A. (2021) Near-surface flow mapping using ADCP records in Minas Passage. *14th European Wave and Tidal Energy Conference*, Plymouth, U.K., September 5-9.

Harding, S., Kilcher, L. and Thomson, J., 2017. Turbulence measurements from compliant moorings. Part I: Motion characterization. *Journal of Atmospheric and Oceanic Technology*, 34(6), pp.1235-1247.

Kammerer, C., Dusek, G., Heilman, L., Kirk, K., and Paternostro, C. (2021) Puget Sound current survey 2015-2017, including the United States' portions of the greater Salish Sea. NOAA Technical Report NOS CO-OPS 093.

Lentz, S.J., Kirincich, A. and Plueddemann, A.J., 2022. A note on the depth of sidelobe contamination in acoustic Doppler current profiles. *Journal of Atmospheric and Oceanic Technology*, 39(1), pp.31-35.

Mantovanelli, A., Cowley, R., Steinberg, C., Heron, S., Williams, D., Spagnol, S. (2014) Quality control of ADCP data with pressure sensor and extraction of the topmost depth strata, Tech. rep., Australian Institute of Marine Science.

Yang, Z., T. Wang, R. Branch, Z. Xiao, and M. Deb, 2021. Tidal Stream Energy Resource Characterization in the Salish Sea. Renewable Energy. 172, 188-208. https://doi.org/10.1016/j.renene.2021.03.028

10 ACKNOWLEDGEMENTS

The project team gratefully acknowledges assistance from Carl Kammerer and Todd Ehret from NOAA in providing raw ADCP data from the CO-OPS survey for sites in the San Juan Islands. Many thanks to Levi Kilcher of NREL for making the connection between CO-OPS and the project team.